Monthly Notices
of the
ROYAL ASTRONOMICAL SOCIETY
MNRAS **467,** 102–114 (2017) doi:10.1093/mnras/stx013

Red supergiant stars in NGC 4449, NGC 5055 (M63) and NGC 5457 (M101)

Sang-Hyun Chun,[1★†] Young-Jong Sohn,[2] Martin Asplund[1] and Luca Casagrande[1]
[1]*Research School of Astronomy and Astrophysics, Australian National University, Canberra, ACT 2611*
[2]*Department of Astronomy, Yonsei University, 120-749 Seoul, Republic of Korea*

Accepted 2017 January 4. Received 2016 December 30; in original form 2016 April 12

ABSTRACT

The photometric properties of red supergiants (RSGs) in three nearby galaxies NGC 4449, NGC 5055 and NGC 5457 were investigated using near-infrared (*JHK*) imaging data obtained from WFCAM UKIRT. The resulting near-infrared photometric catalogue was combined with optical archive data to remove foreground Galactic stars. We found that the foreground stars can be separated from the supergiants in a $(i - K, r - i)$ colour–colour diagram. The $(J - K, K)_0$ colour–magnitude diagrams of the three galaxies are investigated and compared with theoretical isochrones. The majority of RSGs in the three galaxies have common age ranges from $\log(t_{yr}) = 6.9$ to $\log(t_{yr}) = 7.3$, and this indicates that these galaxies have experienced recent star formation within 20 Myr. For NGC 4449 and NGC 5457, the RSGs are spatially correlated with the H II regions, which, however, is not the case for NGC 5055. We were not able to identify a clear metallicity dependence on the colours and the peak absolute magnitudes of the RSGs in the three galaxies. The inaccuracy of our photometric data contributes to the unclear metallicity effect on the colours of RSGs. Instead, we found a similar colour distribution and a constant peak magnitude of $M_K = -11.9$ for the RSGs in the three galaxies. Therefore, we note that additional spectroscopy data for our RSG candidates, including photometry, are necessary to examine whether the RSG population changes with metallicity.

Key words: stars: massive – supergiants – galaxies: photometry – galaxies: stellar content – infrared: stars.

1 INTRODUCTION

Nearby galaxies are ideal objects for studying the mechanisms of galaxy formation and evolution. Their close distances enable individual stars to be resolved in the galaxies, from which the properties of various stellar populations in the galaxies can be investigated. The resolved stellar populations and their spatial distribution provide clues to past galaxy formation history, such as star formation history, stellar substructures (which indicate past merging or accretion events) and effects caused by the environment.

Among the resolved stellar populations in nearby galaxies, massive stars are useful and important sources for investigating the structures and formation of nearby galaxies. Their high masses produce high luminosity; hence, they are easily resolved in the distant galaxies. Therefore, a large sample of massive stars in galaxies provides an excellent test bed to confirm the variation of the stellar evolutionary theory resulting from several physical processes (e.g. mass loss, core overshooting and initial rotation), which determine the evolution of massive stars (Schaller et al. 1992; Charbonnel et al. 1993; Meynet & Maeder 2005; Drout, Massey & Meynet 2012). In particular, these physical processes depend on the stars' initial metallicity (Humphreys 1979; Elias, Frogel & Humphreys 1985; Maeder & Meynet 2001; Vink, de Koter & Lamers 2001); thus, it is important to gather the contents of massive stars for a number of galaxies spanning various metallicities to understand how the processes change according to the chemical abundances of stars. The massive stars also provide an opportunity to investigate the overall evolution and formation of the galaxies themselves. They are mostly younger than ~100 Myr and are associated with a star-formation region; thus, the recent star-formation history and initial mass function in galaxies can be explored. In addition, the massive stars contribute to the chemical enrichment of galaxies through very significant mass loss during their lifetime and supernovae at the end of life (Maeder 1981; Massey 2013). The exact mechanism of mass loss and supernova formation is still unclear. Thus, more sophisticated studies of massive stars are critical for understanding the chemical enrichment of galaxies as well as the mechanism for mass loss and supernova formation of massive stars.

In this study, we focus on the red supergiant stars (RSGs) among the massive stellar populations in nearby galaxies. Moderately massive stars with initial masses of between 9 $M_\odot$ and 25 $M_\odot$ evolve

★ E-mail: shyunc.m@gmail.com
† Visiting researcher at the Research School of Astronomy, Astrophysics.

to the RSG stage in which the core is burning helium. The RSGs are an excellent sample for testing evolutionary theory in the last stage of massive stars because of their unique physical properties and high luminosities. These stars have low effective temperatures ($T_{\rm eff}$ < 4800 K) and very large physical sizes due to the significant expansion of their atmosphere. The resulting low surface gravity produces a huge mass loss between 10^{-8} and 10^{-4} $M_\odot$ yr^{-1} (Massey et al. 2005; Verhoelst et al. 2009; Sargent, Srinivasan & Meixner 2011), which determines their final evolution.

The disagreement between the observational results of RSGs and the predictions of evolutionary theory has been an ongoing challenge in understanding the physical properties of RSGs. Massey & Olsen (2003) and Massey (2003) noted that the effective temperatures and luminosities of RSGs in the Hertzsprung–Russell (H-R) diagram are much cooler and more luminous than evolutionary models predict. This disagreement was initially expected to be a limitation of the models because the RSG atmospheres are too complex and uncertain to be reproduced in theory. However, Levesque et al. (2005) found that the real problem was in the temperature and luminosities inferred from observations. They derived new effective temperatures and luminosities of the Galactic RSGs by fitting moderate-resolution spectrophotometry with the new generation of the MARCS model (Plez 2003; Gustafsson et al. 2003, 2008), and found that the location of RSGs in the H-R diagram was consistent with the evolutionary tracks. The new generation of the MARCS model updated the treatment of the opacity of molecular bands (e.g. TiO), and thus, was able to provide much more accurate effective temperatures for RSGs. However, there is still a possibility that the temperature induced by the TiO lines is unreliable (Levesque et al. 2006). Indeed, a recent study of RSGs in the Magellanic Clouds (Davies et al. 2013) suggests that temperatures from TiO lines are systematically lower than those obtained from the line-free continuum region of spectral energy distributions (SEDs) or the flux integration method. They also noted that the SEDs fitted to TiO lines overpredict the flux in the near-infrared, and finally concluded that TiO lines are not a good indicator of the effective temperatures of RSGs and that the SED method provides better results.

Since the work of Levesque et al. (2005), similar studies of RSGs have been executed in extragalactic galaxies (Levesque et al. 2006; Massey et al. 2009; Drout et al. 2012), and agreement between observations and theory in the H-R diagram has been found. However, previous studies of RSGs in extragalactic galaxies were limited to the Magellanic Clouds and M31 or M33, and the temperature inferred by TiO lines still has uncertainty. Thus, obtaining more complete statistics for the RSGs in nearby galaxies with a wide range of metallicities is critical for examining the physical properties of RSGs. As a first step in the extragalactic research of new RSGs, we select the RSGs in three nearby galaxies NGC 4449, NGC 5055 and NGC 5457. Section 2 introduces the data observations, reduction and photometry. The identification of RSGs in the three galaxies and photometric properties are discussed in Section 3. In Section 4, we compare the colour–magnitude diagrams (CMDs) of the identified RSGs with the theoretical isochrones and investigate their spatial distributions. A summary of the results is given in Section 5.

1.1 NGC 4449

NGC 4449 is at a distance of 3.82 ± 0.18 Mpc (Annibali et al. 2008), and its stellar mass is analogous to that of the Large Magellanic Cloud (LMC). The high Galactic latitude ($b \approx 70°$) of NGC 4449 provides a low foreground extinction and a colour excess of only $E(B - V) = 0.019$ (Schlafly & Finkbeiner 2011). Its abundance of $12 + \log({\rm O/H}) \approx 8.31$ (Talent 1980; Hunter, Gallagher & Rautenkranz 1982; Martin 1997) indicates that the metallicity of this galaxy is comparable to that of the LMC, but its star-formation rate (SFR) is higher. Thronson et al. (1987) estimated the current SFR of ∼1.5 $M_\odot$ yr^{-1}, which makes it one of the strongest starbursts in the nearby Universe. It is notable that NGC 4449 has undergone an external perturbation through substantial interaction with other galaxies. An extended H I halo and ionized gas with complex morphologies, such as filaments and bubbles, were found around NGC 4449 (Hunter & Gallagher 1997; Hunter et al. 1998). The peculiar kinematics of H II regions within the galaxy (Hartmann, Geller & Huchra 1986) also suggests the possibility of an interaction with other galaxies. Indeed, Annibali et al. (2012) discovered a high massive globular cluster with a flattened shape and tidal tails, suggesting that it could be the nucleus of a satellite galaxy disrupted by NGC 4449. In addition, after Karachentsev, Karachentseva & Huchtmeier (2007) first detected the faint stellar stream around NGC 4449, Martínez-Delgado et al. (2012) analysed the red giant branch stars in this stream and discussed the merging of a satellite dwarf galaxy. A detailed study of this galaxy is essential for understanding the possible association between the merging process and a high SFR.

1.2 NGC 5055 (M63)

NGC 5055 is a relatively isolated flocculent spiral galaxy whose distance is in the range from 7.2 to 10.1 Mpc according to previous studies (Pierce 1994; Leroy et al. 2009). In this study, we adopted the distance of 7.9 Mpc given by Tully et al. (2009). A low extinction value of $E(B - V) = 0.016$ was provided by Schlafly & Finkbeiner (2011). The study of oxygen abundance in H II regions by Pilyugin & Thuan (2005) gives $12 + \log({\rm O/H}) \approx 8.59 \pm 0.07$ for this galaxy. NGC 5055 also has ongoing accretion features, such as a hot disc, warps and a stellar tidal stream, around the halo. Battaglia et al. (2006) revealed that the H I gaseous disc is warped and extends out to 40 kpc from the centre. A heated disc (XUV disc) was found in the outskirts of NGC 5055 (Thilker et al. 2007). A stellar stream with low surface brightness was detected by van der Kruit (1979), and using its arc-like structure, Chonis et al. (2011) suggested that this stream originated from an accreted satellite galaxy.

1.3 NGC 5457 (M101)

NGC 5457 is a well-studied face-on spiral galaxy. As it is located at a high galactic latitude ($b \sim 60°$), the foreground extinction is $E(B - V) \approx 0.017$ (Schlafly & Finkbeiner 2011). This is sufficiently small to provide an excellent opportunity to study its massive stars. However, its physical distance remains uncertain with a large range of $(m - M)_0 = 29.04 - 29.71$ (Shappee & Stanek 2011; Matheson et al. 2012; Vinkó et al. 2012). In this study, we assumed that the distance to the galaxy is $(m - M)_0 = 29.045$, as given by Shappee & Stanek (2011). Although several studies indicated a metallicity gradient in the disc (Searle 1971; Sedwick & Aller 1981; Garnett & Kennicutt 1994), the oxygen abundance in the central region is $12 + \log({\rm O/H}) \approx 8.76$ (Kennicutt, Bresolin & Garnett 2003). Like NGC 5055, the complicated arm structure and highly asymmetric disc morphology suggest previous accretion or interactions with other galaxies (Waller et al. 1997). An extended and distorted H I disc (van der Hulst & Sancisi 1988; Walter et al. 2008) and extended UV emission in the outer disc (Thilker et al. 2007) also support recent accretion and interaction.

Table 1. Observational log.

Galaxy	Filter	Exposure time (N × micro-step × dither × seconds)	(FWHM) (arcsec)
NGC 4449	J	2 × 4 × 5 × 20 s	0.84
	H	2 × 9 × 5 × 20 s	0.85
	K	2 × 9 × 5 × 20 s	0.84
NGC 5055	J	2 × 4 × 5 × 20 s	0.96
	H	2 × 9 × 5 × 20 s	0.92
	K	2 × 9 × 5 × 20 s	0.96
NGC 5457	J	2 × 4 × 5 × 20 s	0.72
	H	2 × 9 × 5 × 20 s	0.55
	K	2 × 9 × 5 × 20 s	0.87

2 OBSERVATION, DATA REDUCTION AND PHOTOMETRY

2.1 Near-infrared imaging data of UKIRT

Near-infrared *JHK* imaging data of the three galaxies were obtained from the WFCAM detector mounted on the UKIRT telescope in Hawaii during the nights of 2013 April. The WFCAM camera consists of four 2048 × 2048 Rockwell Hawaii-II (HgCdTe) arrays with a 12.83 arcmin gap between the arrays. One camera provides a field of view of 13.65 × 13.65 arcmin with a spatial resolution of 0.4 arcsec pix^{-1}, and the four tiles observation provides a continuous sky of 0.75 square degrees. The galaxies were alternately observed on cameras 2 and 3 of the WFCAM arrays, and the corresponding camera on which the galaxies were not placed was used as a blank sky field to correct for thermal background emission. A five-point dithering observation with an individual exposure of 20 s was used, and given one dithered position, a micro-stepping observation (2 × 2 for J and 3 × 3 for HK) was applied to obtain well-sampled stars. Table 1 presents the observational log for the target galaxies.

The standard data reduction processes (dark subtraction, flat-fielding and crosstalk removing) were done by the pipeline of the Cambridge Astronomy Survey Unit (CASU). We made the blank sky images by median-combining the CASU-processed images of the sky field and subtracted them from all target images. The residual background level was also subtracted. All sky-subtracted images of galaxies in camera 2 and camera 3 were separately combined into two single images using the SWARP program (Bertin et al. 2002). In addition, we combined adjacent camera images into separate single images, which acted as a control field in estimating the contamination of field stars and background galaxies in the target field (see Section 3). The average seeing condition in the final images is between 0.8 and 1.0 arcsec, and these values are summarized in Table 1.

The point spread function (PSF) fitting routine of DAOPHOT II/ALLSTAR (Stetson 1987; Stetson & Harris 1988) was applied to measure the instrumental magnitude of stars in the three galaxies. We selected 30–50 bright and isolated stars for each galaxy to construct the PSF, and its quality was improved by removing neighbouring stars around the PSF stars and reconstructing the PSF iteratively. The equatorial coordinates of the stars on the detector were calculated using the reference stars of the 2MASS point-source catalogue. We transformed the instrumental magnitudes into the 2MASS filter system using the colour term between the WFCAM and 2MASS systems (Dye et al. 2006) and then calibrated the photometric zero levels with respect to the 2MASS catalogue. The calibrated stellar magnitudes of each galaxy in camera 2 and camera 3 were combined into a single catalogue in which we adopted the weighted mean magnitude for the duplicated stars. Finally, we resolved 2859 stars for NGC 4449, 1876 stars for NGC 5055 and 3850 stars for NGC 5457. Then, we estimated the completeness fraction in the final photometric measurements by performing artificial star experiments. For the sources of NGC 4449, we note that stars with $K = 19.5$ have ∼80 per cent completeness. For the stars of the distant galaxies (NGC 5055 and NGC 5457), the ∼70 per cent completeness encounters near $K = 19.4$ (NGC 5055) and 19.0 (NGC 5457) across the galaxies.

Table 2. Supplementary archive imaging data used in this study.

Galaxy	Telescope	Filter	Exposure time	FWHM (arcsec)
NGC 4449	Subaru	r'	10 s, 5 × 45 s	0.52
		i'	10 s, 5 × 45 s	0.50
NGC 5055		R	4 × 60 s, 12 × 180 s	0.80
		I	4 × 60 s, 4 × 240 s	0.58
NGC 5457	CFHT	r'	2000 s	0.76
		i'	3690 s	0.75

2.2 Supplementary optical imaging data from archives

We searched optical imaging data of our galaxies from several public archives to remove the foreground Galactic stars and background distant galaxies in our galaxy field (see Section 3). In this section, we summarize the basic information of the archive data we used, the reduction process and photometry.

We used *ri*-band and *RI*-band Suprime-Cam images from the Subaru archive (SMOKA; Baba et al. 2002) for NGC 4449 and NGC 5055, respectively. The raw images and associated calibration images were obtained and then reduced using the Suprime-Cam Deep Field Reduction package 2 (SDFRED2). For NGC 5457, the pre-processed *ri*-band images of the Canada-France-Hawaii Telescope Legacy Survey (CFHTLS) were used. The seeing conditions of the archive images are between 0.5 and 0.8 arcsec, and an overview of the archive data we used is provided in Table 2. The PSF photometry for all archive images was done using the DAOPHOT II/ALLSTAR program (Stetson 1987; Stetson & Harris 1988). The instrumental magnitudes of NGC 4449 and NGC 5055 were then calibrated into a standard system using the SDSS catalogue. We note that the *RI* magnitude of NGC 5055 was first transformed into a *ri* band of the SDSS system based on the empirical relations of Jordi, Grebel & Ammon (2006). The APASS DR 8 star catalogue was used to calibrate the magnitude of NGC 5457. Finally, the photometric measurements in the overlapped region of our UKIRT field area were used in the following analysis.

3 COLOUR–MAGNITUDE DIAGRAM AND IDENTIFICATION OF SUPERGIANT STARS

The ($J - K$, K) CMDs of the resolved stars in the three galaxies are compared in Fig. 1. We also present the CMDs of the stars in the control fields to evaluate the contamination by the field stars and background galaxies in the galaxy field. In the CMDs of the galaxies, the most prominent component is the RSG population in the colour range $0.9 \le (J - K) \le 1.5$, while this population almost disappears in the CMDs of the control field. It is also apparent that there is a population of stars that form a vertical sequence near $(J - K) \sim 0.9$. These stellar objects are most likely foreground Galactic dwarfs, and they are more distinct in the CMDs of the

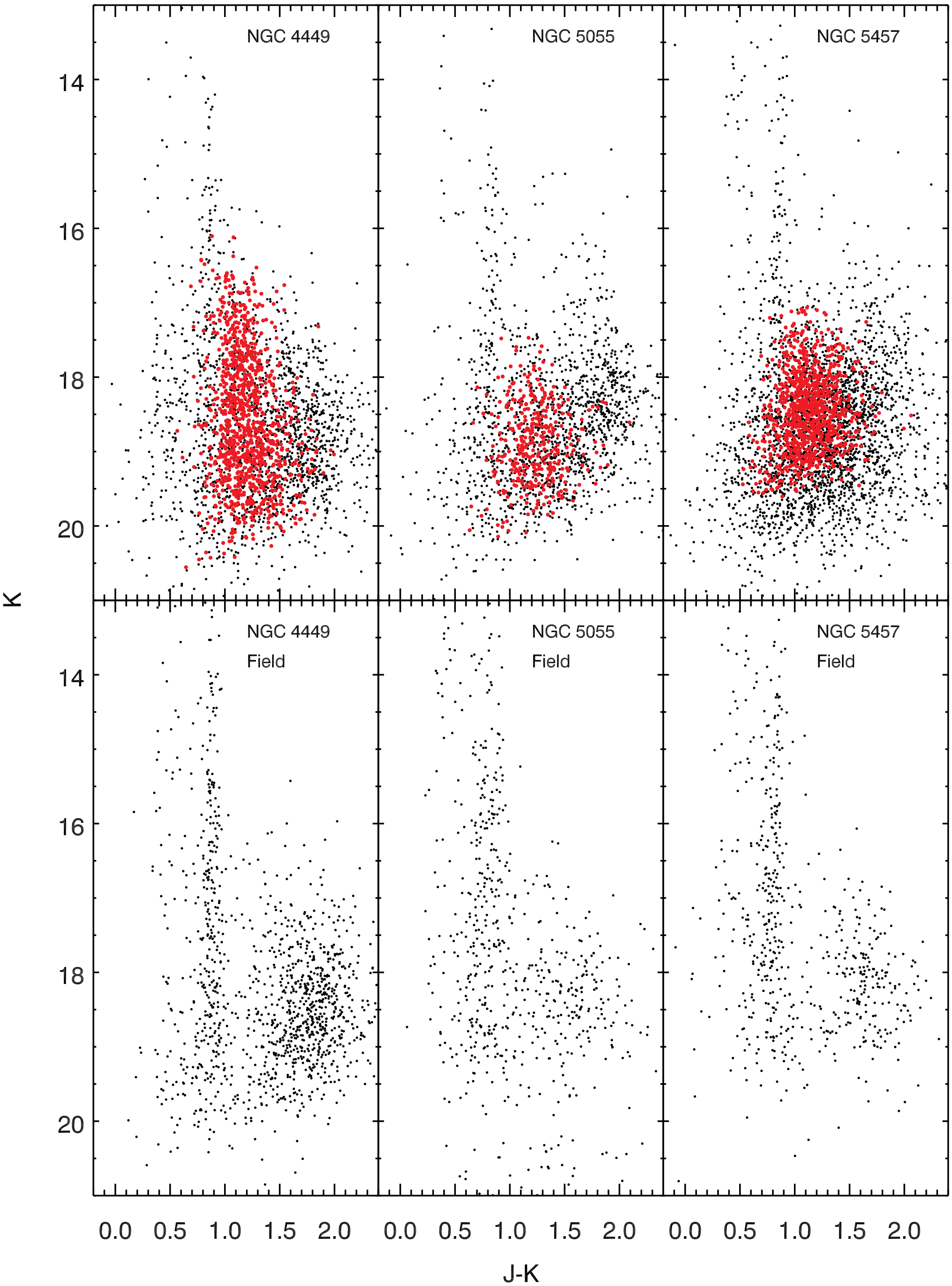

Figure 1. ($J-K$, K) colour–magnitude diagram for the three galaxies (upper panels) and control fields (lower panels). The selected supergiant candidates are plotted as red dots in the upper panels.

control fields. In addition, another population with a broad colour distribution appears in the red-coloured region, i.e. $(J-K) \geq 1.5$. This group is a composition of distant background galaxies, and the CMDs of the control field clearly better define this population. The bright asymptotic giant branch (AGB) stars are also shown in the CMD of NGC 4449.

The separation of RSGs from foreground stars has been a primary issue in the study of supergiants. As clearly shown in Fig. 1, the RSG populations in the three galaxies are significantly contaminated by the foreground dwarf stars, background galaxies and even bright AGB stars. Therefore, an accurate identification of the RSG population is essential. Massey (1998) used a ($B-V$, $V-R$) colour–colour diagram to distinguish RSGs from the foreground stars, as the $(B-V)$ colour is a sensitive indicator of the surface gravity at low effective temperature, while the $(V-R)$ colour reflects the effective temperature. In the ($B-V$, $V-R$) colour–colour diagram, supergiant stars have a larger $(B-V)$ colour at a given $(V-R)$ than that of foreground dwarf stars. Several recent

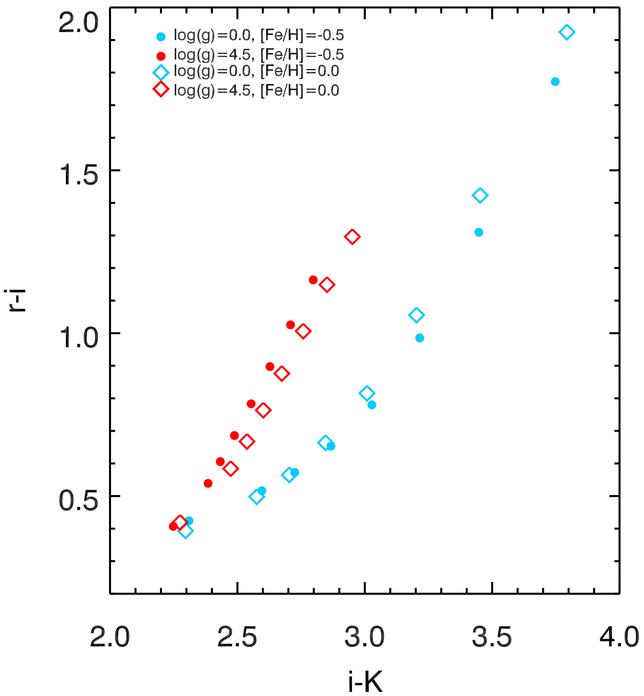

Figure 2. Expected $(i - K, r - i)$ colour–colour distribution of RSGs ($\log g \sim 0.0$) and foreground dwarfs ($\log g \sim 4.5$). The MARCS model with several temperature ranges (3400–4250 K) and two metallicities ([Fe/H] = −0.5, 0.0) was used to derive the expected colours. The temperature increases by 100 K to 4000 K, and then by 250 K.

studies (Massey et al. 2009; Drout et al. 2012) of supergiants of the galaxies in the Local Group also identified the RSGs from the foreground dwarfs using the $(B - V, V - R)$ colour–colour diagram. We also followed the strategy used in previous studies and examined the colour–colour diagram. In this study, however, we used the $(r - i, i - K)$ diagram. We first inspect the expected colour values of foreground dwarf and supergiants stars in the $(r - i, i - K)$ diagram using the MARCS model with a temperature range of 3400–4250 K, with $\log g$ values of 4.5 (dwarf) and 0.0 (RSGs), and with two metallicities ([Fe/H] = −0.5 and 0.0) in Fig. 2. The response functions of the 2MASS system (Cohen, Wheaton & Megeath 2003) and SDSS system (Doi et al. 2010), and the photometric zero-points reported by Casagrande & VandenBerg (2014) were used in the colour computation.

As shown in Fig. 2, although the deviation in colours between the two populations decreases as the colour decreases, it is apparent that RSGs are decontaminated from the foreground dwarfs in the red region of the $(r - i, i - K)$ diagram. Thus, we combined and cross-matched our photometry data with the photometric catalogue of supplementary optical imaging data, as explained in Section 2. Then, we excluded the stellar objects for which the measurement errors in the optical and near-infrared bands exceed 0.1 mag. We also rejected the stars with $\chi > 2.0$ and |SHARP| > 2.0 given by ALLSTAR, and thus, we were able to remove the objects near the faint limit of the data. Finally, we obtained 2117 stars for NGC 4449, 1126 stars for NGC 5055 and 1886 stars for NGC 5457 in the near-infrared and optical data.

The left-hand panel of Fig. 3 shows the $(r - i, i - K)$ colour–colour diagram for the resolved stars in NGC 4449. The distribution of stars in NGC 4449 in the colour–colour diagram shows two distinct stellar groups, and this is almost the same as shown in Fig. 2. The reddening vector is almost parallel to the stellar distribution, and thus, it does not significantly affect the distribution of the stars on the colour–colour diagram, given the low $E(B - V)$ of ∼0.2 for the three galaxies. We found that foreground dwarf stars form a thin stream with a larger value in $(r - i)$ at a given $(i - K)$, while supergiant stars show a broad distribution of colours due to the photometric error and the mix of AGB stars and background galaxies. The solid line in the left-hand panel of Fig. 3 is a cut-off between supergiant stars and foreground dwarfs. We selected the stars below the cut-off line as preliminary supergiant candidates. We note that, as shown in Fig. 2, the separation between foreground dwarfs and supergiants in $(i - K) < 2.1$ and $(r - i) < 0.4$ of the $(i - K, r - i)$ colour–colour diagram is not obvious. Thus, we just filtered the stars with $(i - K) < 2.1$ from the supergiant candidates to reduce contamination. The cut-off lines between supergiants and dwarfs for the other two galaxies are like that of NGC 4449.

Although we sorted the foreground dwarfs using the $(r - i, i - K)$ colour–colour diagram, there are still distant background galaxies in the sample of pre-selected supergiant stars. We examined colour–colour diagrams using various filter combinations to filter out the background galaxies and found that in $(r - H) - (H - K)$ and $(r - K)$ colour–colour diagrams, most supergiant candidates show a one-dimensional distribution, while the galaxies deviate from the linear distribution. The right-hand panel of Fig. 3 shows the stellar distributions of NGC 4449 in the $(r - H) - (H - K)$ and $(r - K)$ colour–colour diagram, and we note here that the colour–colour diagrams of the remaining two galaxies also showed a similar tendency. The linear fit to the supergiant candidates is described by a solid line, and the absolute differences (Δd) of the points from this fit were calculated. For the three galaxies, we selected the stars with $\Delta d \leq 1.0 \sim 2\sigma$, where σ is the standard deviation of the absolute difference. We were able to select 1053 supergiants (including bright AGBs) for NGC 4449, 354 supergiants for NGC 5055 and 941 supergiants for NGC 5457. Finally, we estimated the residual contamination rate in our selected supergiants by comparing the number densities of supergiants and control field stars on the $(J - K, K)$ CMDs. The number densities of supergiants and control field stars on the CMDs are measured in various colour and magnitude bins. If we assume that the stars in the area where the number densities of control field stars are larger than those of supergiants on CMDs that are contaminated by foreground dwarfs or distant galaxies, the numbers of contaminated stars in our sample of selected supergiants are 91 (∼9 per cent) for NGC 4449, 20 (∼6 per cent) for NGC 5055 and 31 (∼3 per cent) for NGC 5457.

The selected supergiants are superimposed in the $(J - K, K)$ CMDs of Fig. 1. Some supergiants in the transition phase from the blue region to the RSG stage or from the RSG to the blue side appear in the blue-coloured region of the CMDs. However, we also caution that these stars are probably foreground dwarf stars because they are placed on the branch of foreground dwarf stars on the $(J - K, K)$ CMDs. Thus, we classified the stars with $(J - K) < 0.9$ as possible RSGs among the identified RSG candidates. The stars redder than $(J - K) = 1.3$ are expected to have a substantial amount of dust, and hence the adopted reddening values in this study may be underestimated. Therefore, we also classified these stars as possible RSG candidates.

4 DISCUSSION

We identified the RSG candidates for the three galaxies by examining the observed and theoretical $(r - i, i - K)$ colour–colour diagrams. In this section, we compare the locations of RSG candidates of the three galaxies in the $(J - K, K)_0$ CMDs with the

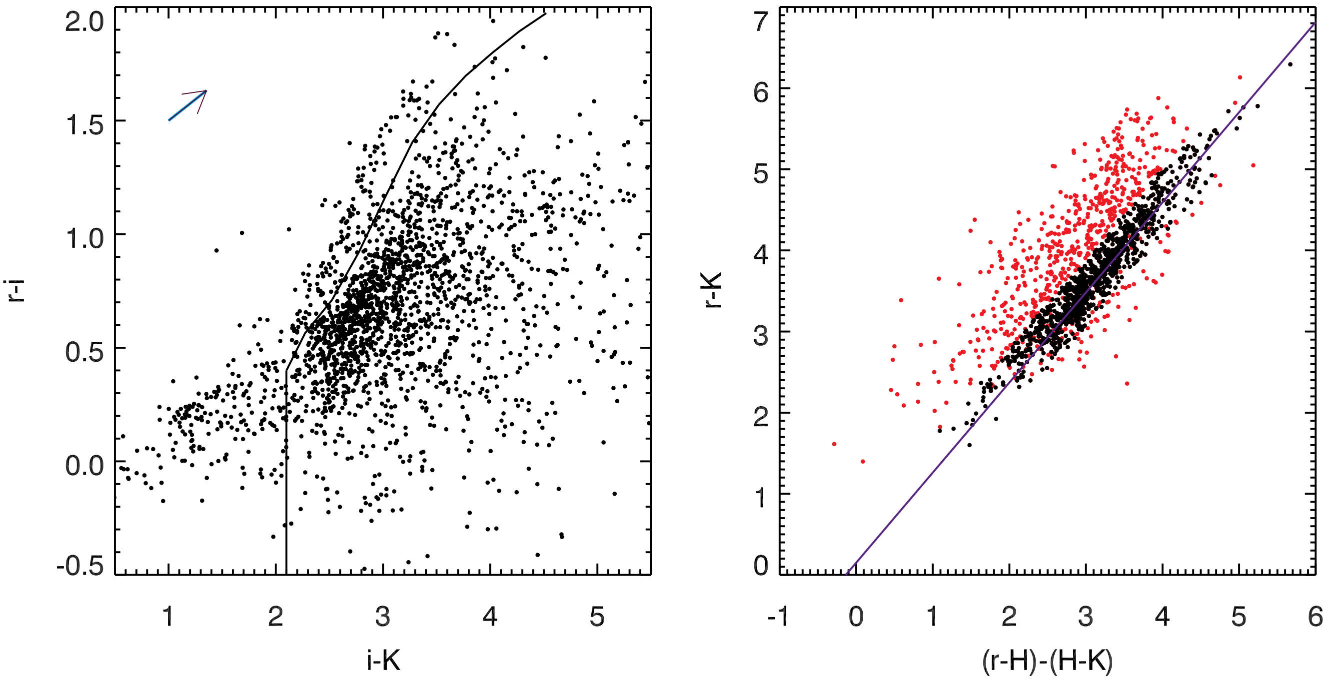

Figure 3. Left: $(i-K, r-i)$ colour–colour diagram for the resolved stars in NGC 4449. The solid line is an adopted dividing line to separate foreground dwarfs and RSGs. Stars with larger $(r-i)$ values at a given $(i-K)$ are foreground dwarf stars. The reddening vector is indicated by the arrow. Right: $(r-H)-(H-K)$ and $(r-K)$ colour–colour diagram for the pre-selected supergiant stars in NGC 4449. The solid line indicates a one-dimensional linear fit to the supergiants. The red dots are excluded as background galaxies and a few outliers from the selection criteria.

theoretical isochrones of PARSEC (Bressan et al. 2012, 2013). When we compare the identified RSGs and theoretical isochrones, the Galactic extinction and additional extinction around RSGs are corrected because the RSGs produce significant dust through their winds. We adopted average reddening values obtained from the H II region of each galaxy, since several studies (Drout et al. 2012; Neugent et al. 2012) adopted the reddening values for the RSGs from early-type stars. Indeed, the RSGs show a spatial correlation with the H II region in our analysis. Thus, the adopted additional reddening values are $E(B-V) = 0.18$, 0.26 and 0.23 for NGC 4449 (Hill et al. 1998), NGC 5055 (Rozas 2008) and NGC 5457 (Rosa & Benvenuti 1994), respectively. We also examine the spatial distributions of the selected RSGs with the Hα image to investigate the spatial correlation between the sky position of RSGs and H II regions. The H II regions in the galaxies are highly related with recent star formation, but the formation history in each H II region is complex and variable. Thus, we compare the CMDs of RSGs within the H II regions, even though the Hα emission traces the most recent ($\leq$10 Myr) star formation.

4.1 NGC 4449

The $(J-K, K)_0$ CMD of RSGs in NGC 4449 is shown in the top-left panel of Fig. 4. We present the genuine RSGs and possible RSGs as black and blue dots, respectively. The theoretical isochrones with $Z = 0.006$ and several ages of $\log(t_{yr}) = 6.9$, 7.1, 7.3, 7.5 and 8.0 were used to compare the location of the stars. In the faint magnitudes, the bright AGB stars older than 100 Myr were resolved in our observation and compared with the isochrone with an age of $\log(t_{yr}) = 8.0$. The peak magnitude of the isochrone with $\log(t_{yr}) = 8.0$ is about $K_0 = 18.94$ ($M_K \approx -8.9$), and thus, we assigned the stars below this magnitude as AGBs and they are indicated as grey points in Fig. 4. We note that our boundary magnitude between RSGs and AGBs is comparable to that of Davidge (2010) in their study of NGC 253. It is apparent that the isochrones with metallicity $Z = 0.006$ give a good match to the genuine RSGs in NGC 4449. The majority of RSGs in the galaxy are broadly distributed between the isochrones with age range $\log(t_{yr}) =6.9$–7.5, and this indicates that NGC 4449 experienced star formation as recently as 30 Myr ago. However, some RSGs are older than $\log(t_{yr}) = 7.5$, and thus, the upper age limit of RSGs in NGC 4449 seem to be about $\log(t_{yr}) = 8.0$ ($\sim$100 Myr). There are some stars younger than $\log(t_{yr}) = 6.9$ in the brightest magnitude.

The sky positions of RSG candidates along with an Hα image are shown in the top-right panel of Fig. 4. We used the F658N (Hα) of an *HST*/ACS image obtained by Annibali et al. (2008), who found that young stars of NGC 4449 between 10 and 100 Myr old are distributed along the S-shaped structure centred on the galaxy nucleus. We also found similar features in the spatial distribution of detected RSGs. Although the RSGs broadly spread out to the outskirts of the H II disc, they show a distorted shape and extended structure in the north–south direction. In particular, RSGs appear in clump structures around the H II regions, showing a correlation with the H II regions. As Annibali et al. (2008) suggested, this structure could be a bar, which is a common feature among Magellanic irregular galaxies.

From the spatial distribution of RSGs, we found the spatial correlation between the RSGs and the H II regions. Four H II regions, 0.5 arcmin in radius, were selected (A, B, C and D in the Hα image), and the CMD of each region is plotted in the bottom panel of Fig. 4. We note that the genuine RSGs are used in the bottom panel of Fig. 4. The isochrones from the top-left panel are superimposed. Although the four regions commonly have RSGs in the age range between $\log(t_{yr}) = 6.9$ and 7.5, the most luminous parts in the CMDs are different. It is notable that the C and D regions have several luminous RSGs, whose ages are about $\log(t_{yr}) = 6.9$,

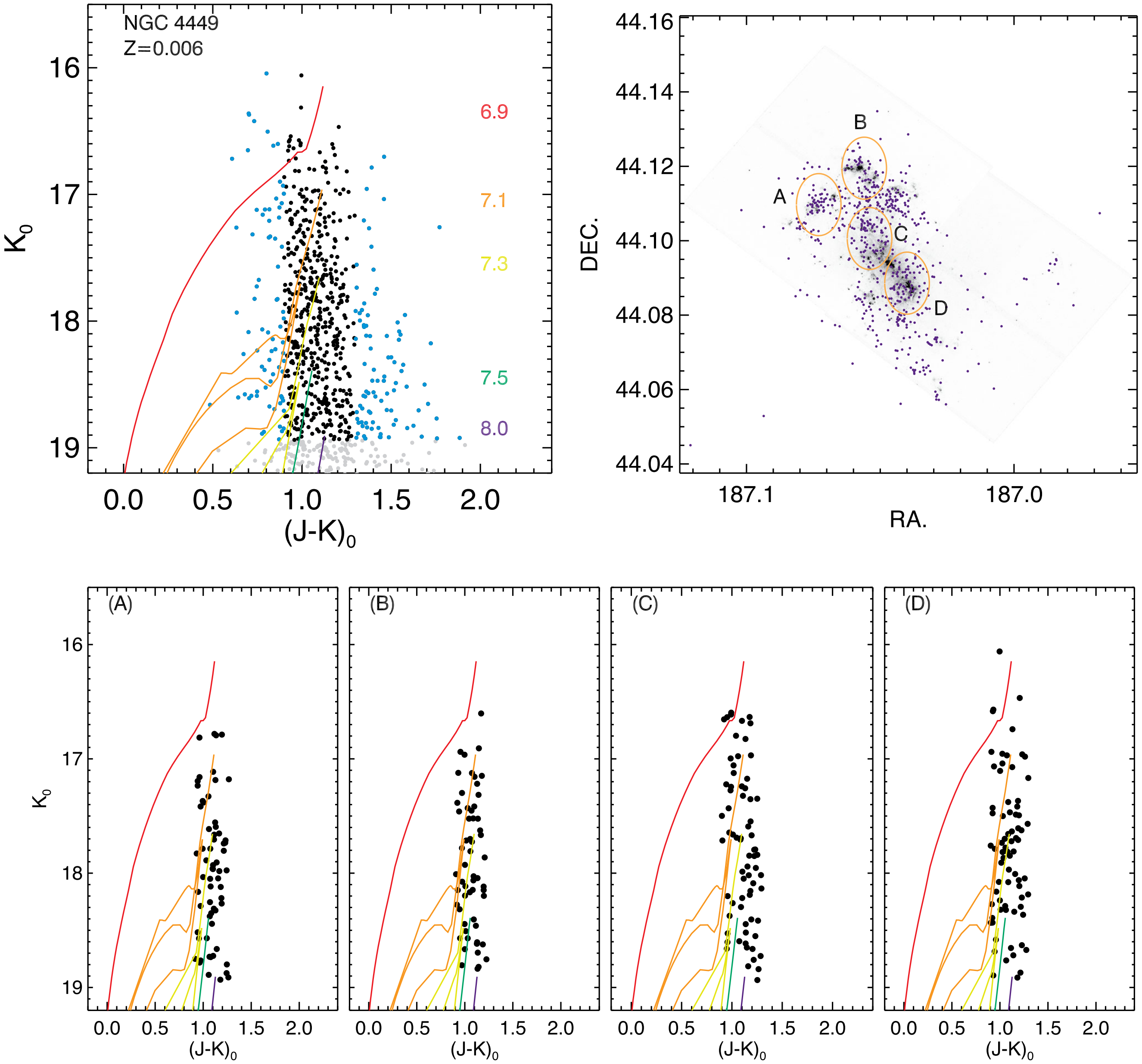

Figure 4. Top left: $(J - K, K)_0$ CMD of the RSGs in NGC 4449. Blacks dots indicate the selected genuine RSGs in Section 3, blue points are possible RSGs and grey points represent the AGBs in NGC 4449. The theoretical isochrones with ages of log = 6.9, 7.1, 7.3, 7.5 and 8.0 are shown as solid lines with different colours. Top right: Spatial distribution of the RSGs (blue dots) of NGC 4449 over an ACS-F658N (Hα) image in a grey-scale. Four H II regions (A, B, C and D), 0.5 arcmin in radius, are indicated. Bottom: $(J - K, K)_0$ CMDs of RSGs in the four H II regions shown in the Hα image. The possible RSG candidates are not included in the lower panels. The label in each panel corresponds to the selected H II region. The theoretical isochrones are the same as those of the top-left panel.

while stars younger than $\log(t_{yr}) = 6.9$ do not appear in the A and B regions. Therefore, the H II regions (C and D) of the galaxy nucleus are likely to have more luminous and young massive RSGs than in the outskirts (A and B) of the galaxy, indicating that recent star formation is not uniform over NGC 4449.

4.2 NGC 5055 (M63)

We plotted the $(J - K, K)_0$ CMD of RSGs in NGC 5055 with theoretical isochrones with $Z = 0.008$ and ages of $\log(t_{yr}) = 6.9$, 7.1 and 7.3 in the top-left panel of Fig. 5. The possible RSGs are represented by blue dots, and they are placed on the blue and red side of the genuine RSGs. The isochrones with ages of $\log(t_{yr}) = 6.9$–7.3 match well with the main sequence of the RSGs of NGC 5055, indicating that there has been recent star formation within 20 Myr. Although rejecting stars with larger photometric errors and χ and SHARP values results in a small number of stars at the faint magnitude, the 50 per cent completeness limit still indicates the possibility that several RSGs older than $\log(t_{yr}) = 7.3$ are not detected in our observation. The most luminous stars ($K_0 = 17.5$–17.6) are younger than $\log(t_{yr}) = 6.9$.

The top-right panel of Fig. 5 shows the spatial distribution of RSGs. We adopted the Hα image from the Local Volume Legacy (Kennicutt et al. 2008; Dale et al. 2009) and explored the spatial

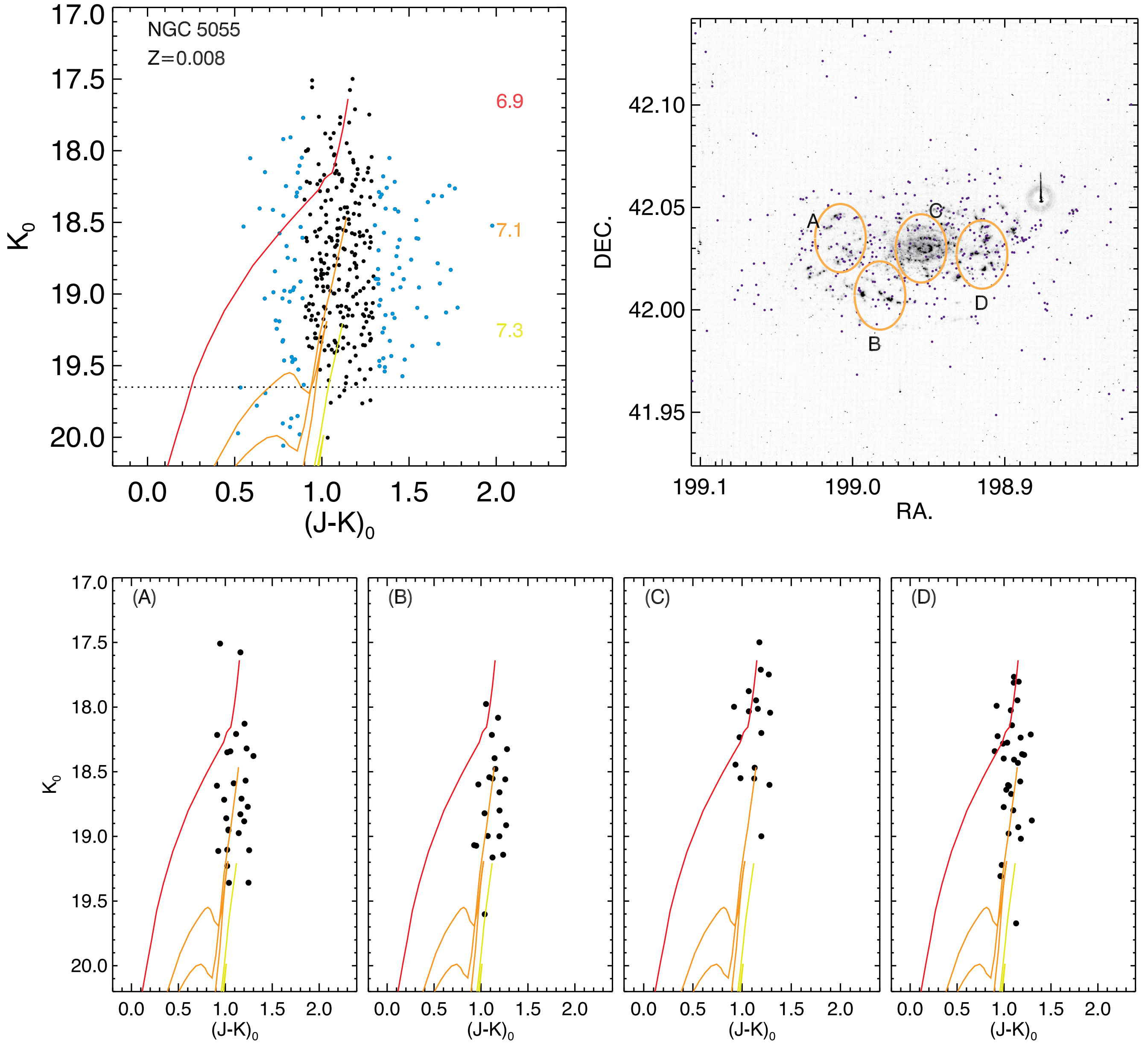

Figure 5. Top left: $(J - K, K)_0$ CMD of the RSGs in NGC 5055. The black and blue dots represent the genuine RSGs and possible RSG candidates, respectively. We compared the distribution of RSGs in the CMD with the theoretical isochrones of $Z = 0.008$ and several ages, which are indicated by solid lines with different colours. The dotted line indicates the 50 per cent completeness limit in the K magnitude. Top right: Spatial distribution of RSGs in NGC 5055 compared with an Hα image. Four H II regions (A, B, C and D), 1.0 arcmin in radius, are indicated. Bottom: $(J - K, K)_0$ CMDs of RSGs in the four regions shown in the Hα image. The label in each panel corresponds to the selected H II region. The isochrones are the same as those of the top-left panel.

correlation between the RSGs and H II regions. The distribution of RSGs shows that the RSGs of NGC 5055 are likely to be along the spiral arms. However, a tight spatial correlation between the RSGs and H II regions does not appear, unlike for NGC 4449. We could not find definite clumpy structures of RSGs; rather, the RSGs seemed to be broadly distributed to the outskirts of the galaxy. Although Chonis et al. (2011) found complex and faint stellar light in the outer halo of NGC 5055, including a large stellar stream, its red colour (Chonis et al. 2011) suggests that the diffuse stellar haloes are dominated by an old stellar population, and thus, the extended distribution of RSGs in this study is not likely to have a direct association with the faint stellar structures in the outer halo of the galaxy. Interestingly, Chonis et al. (2011) also noted long and clumpy filaments (features g and h in their figs 9 and 10) in the outskirts of the disc from the H I map of Battaglia et al. (2006) and the *GALEX* ultraviolet image of Gil de Paz et al. (2007). The blue coloured property of the features suggests that the stellar populations in these features are younger than the tidal stream, indicating that there is no association between the tidal stream feature and the blue extended features. Therefore, the extended distribution of the RSGs in this study may be related to these young structures. Although the sky area of our detection is too narrow to identify a definite spatial correlation of RSGs with the H I map or the *GALEX* ultraviolet image, we indeed found that some of the RSGs in the outskirts of the disc are distributed along part of the long and clumpy features g and h presented by Chonis et al. (2011). Additional exploration using a

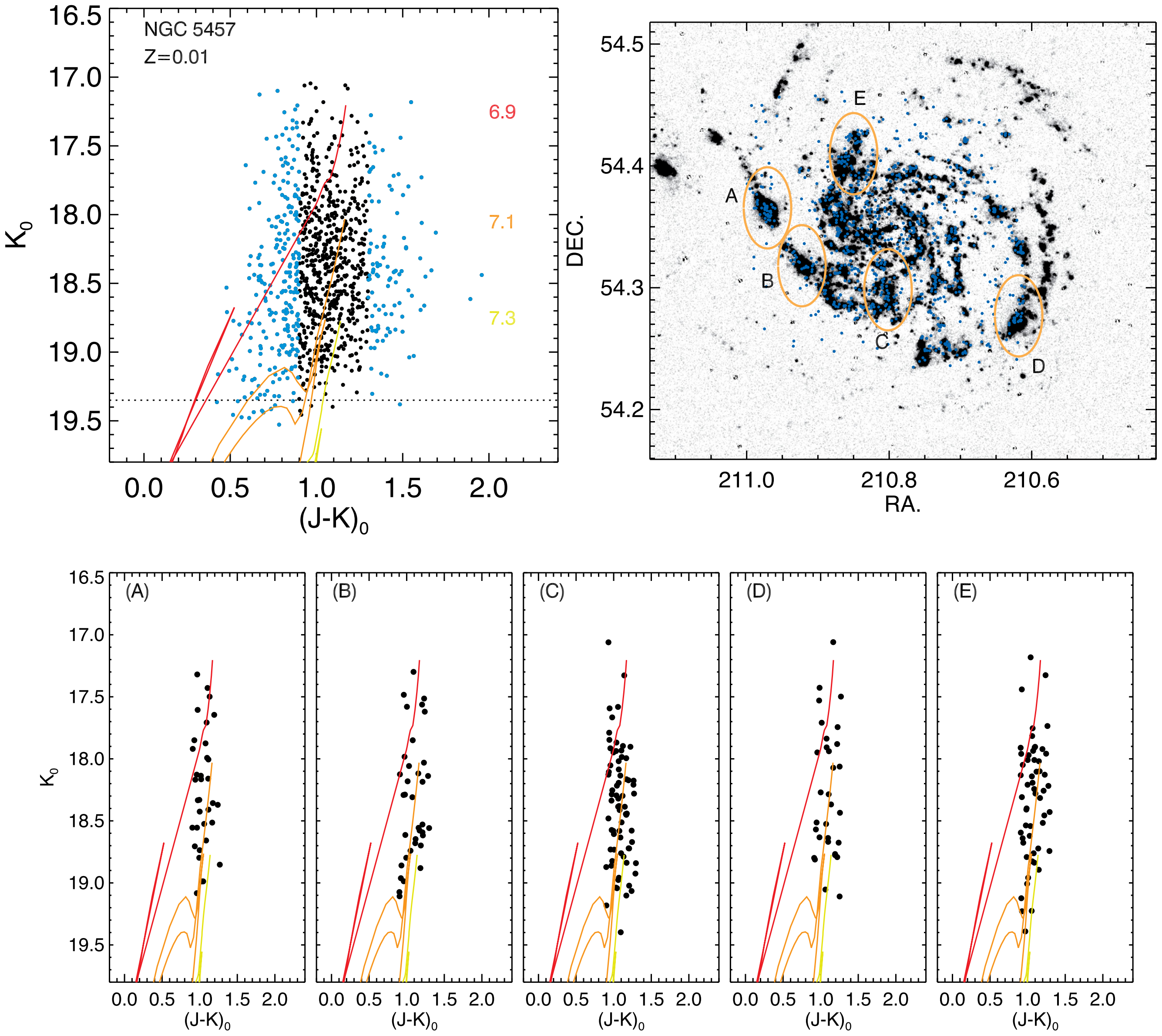

Figure 6. Top left: $(J-K, K)_0$ CMD of the RSGs in NGC 5457. The black and blue dots represent the genuine RSGs and possible RSG candidates. The theoretical isochrones of $Z = 0.01$ and age of $\log(t_{yr}) = 6.9$, 7.1 and 7.3 are shown by solid lines with different colours. The 50 per cent completeness limit is indicated by the dotted line. Top right: Spatial distribution of RSGs (blue points) of NGC 5457 over an Hα image in a grey-scale. Five giant H II regions (A, B, C, D and E), 1.0 arcmin in radius, are indicated. Bottom: $(J-K, K)_0$ CMDs of RSGs in the regions shown in the Hα image. The label in each panel corresponds to the selected H II region. The isochrones are the same as those of the top-left panel.

telescope with a wider field of view and a higher spatial resolution is necessary to find the link between the young stars and the blue extended features.

We selected four regions where the emission of Hα is dominant (A, B, C and D, in the Hα image), and $(J-K, K)_0$ CMDs of genuine RSGs from inside the circle with 1 arcmin radius centred on each region are plotted in the bottom panels of Fig. 5. Although RSGs in the four regions follow the theoretical isochrones with ages between $\log(t_{yr}) = 6.9$ and 7.3, and have similar colours, the magnitudes of RSGs show various distributions depending on the region. The centre of the galaxy (region C) contains more bright RSGs with age $\log(t_{yr}) = 6.9$ than other regions. Considering that the most dominant Hα emission is in the centre of the galaxy, the presence of numerous bright stars and recent star formation in this area are not surprising. We could not find stars below about $K_0 = 18.5$ in the centre, but the low number of RSGs at the faint magnitude seems to be affected by the crowding effect. With the exception of the two brightest RSGs in the A region, the A and B regions seem to have less bright RSGs compared to the other regions. In these regions, the majority of RSGs are older than $\log(t_{yr}) = 6.9$, and only two stars in region A are younger than the $\log(t_{yr}) = 6.9$ isochrone.

4.3 NGC 5457 (M101)

The top-left panel of Fig. 6 shows the distribution of the RSGs in NGC 5457 in the $(J-K, K)_0$ CMD. We also compared the RSGs in the CMD with the PARSEC isochrones with $Z = 0.01$ and several ages of $\log(t_{yr}) = 6.9$, 7.1 and 7.3. It is apparent that NGC 5457 has dominant RSG populations that are distributed between the $\log(t_{yr}) = 6.9$ and 7.3 isochrones. In particular, this galaxy has more RSGs younger than $\log(t_{yr}) = 6.9$ compared with the other two galaxies. As for NGC 5055, the 50 per cent completeness limit of NGC 5457 also shows that there may be further RSGs older than $\log(t_{yr}) = 7.3$ in this galaxy. The blue possible RSG candidates also show a more substantial distribution than the other two galaxies. This is consistent with the active and complex star formation of several giant H II regions in this galaxy.

The sky positions of RSGs in NGC 5457 are shown in the top-right panel of Fig. 6. The Hα image from the Local Volume Legacy (Kennicutt et al. 2008; Dale et al. 2009) was used to compare the RSGs and H II regions. It is evident that the RSGs in NGC 5457 manifest density enhancement in the spiral arms and a strong coherence with the H II region, with a clumpy structure inside the H II region. The clumpy structure of the RSGs in the H II region is also in agreement with the spatial distribution of RSGs reported by Grammer & Humphreys (2013). Thus, the H II regions of NGC 5457 contain not only very young stars with an age of ≈10 Myr but also evolved stellar populations with an age of <100 Myr. We could not find an extended distribution of RSGs to the outskirts of the disc in contrast to the other two galaxies, which show an extended distribution of RSGs. Thus, the recent star formation of NGC 5457 is dominated by the physical properties of the H II region, not by previous merging or accretion events.

Several giant H II regions with spectacular star formation are known in NGC 5457. We selected five giant H II regions (A, B, C, D and E) in the Hα image and investigated the $(J - K, K)_0$ CMD of genuine RSGs in each region. The regions A, B, C and D correspond to the brightest and largest giant H II regions NGC 5462, NGC 5461, NGC 5458 and NGC 5450, respectively. We used stars within 1 arcmin radius centred on each region, and the CMDs are plotted in the bottom panels of Fig. 6. The RSGs in the five regions have the same magnitude ranges, between $K_0 = 17.0$ and $K_0 = 19.0$, and similar colour values. The isochrones with ages between $\log(t_{yr}) = 6.9$ and $\log(t_{yr}) = 7.3$ are matched with the sequences of RSGs. Region C has dominant RSG populations compared to the other regions. To test more precisely the differences between the stellar populations in the giant H II regions, additional high-resolution data and information about very young stellar populations, such as blue supergiants, are necessary. Grammer & Humphreys (2013) examined the stellar populations in several giant H II regions of NGC 5457 using a *HST*/ACS Wide Field Camera image. They found that all giant H II regions have evolved stellar populations (≈40 Myr), and NGC 5461 and NGC 5462, which are discussed in this study, show statistically significant differences in the spatial distribution between young and evolved stellar populations.

4.4 Effect of metallicity on the evolution of RSGs

Metallicity is one of the important factors in determining the evolution of RSGs in CMDs, and the effect of metallicity on RSGs has been examined in several studies. Elias et al. (1985) first noted that as metallicity decreases, the average spectral types of the RSG populations shift to an earlier type. This trend is clearly detected in several galaxies with various metallicities in the Local Group. Massey & Olsen (2003) investigated the RSGs in the Milky Way, LMC and Small Magellanic Cloud (SMC) and found that the distribution of spectral types was skewed towards an earlier spectral type. More recently, Drout et al. (2012) used spectroscopic data for RSGs in M33, which is known to have a significant metallicity gradient, and found that the RSGs in the outskirts of M33 systematically have a higher temperature than those in the inner part of the galaxy.

Elias et al. (1985) attributed the shift of spectral type with metallicity to the varying location of the Hayashi limit (Hayashi & Hoshi 1961) with metallicity. The Hayashi limit is the coolest temperature at which a star can stay in hydrostatic equilibrium and is sensitive to the metallicity: a decrease in the number of heavy elements that provide free electrons results in a decrease in opacity at the surface of stars and subsequently an increase of effective temperature. The RSGs are so large and cool that their location (temperature and luminosity) in the H-R diagram is constrained by the Hayashi limit. Thus, as the Hayashi limit shifts to a warmer temperature with decreasing metallicity, the RSGs also have a higher effective temperature. In addition, this spectral type shift can be also explained by the effect of the low metallicity of the stars: the weak TiO lines at lower metallicities yield earlier spectral types. By comparing the evolutionary tracks for the Milky Way, LMC and SMC, Levesque et al. (2006) stated that the variation of the TiO lines is a secondary effect in the spectral shift and that the main reason is the variation of the Hayashi limit with metallicity. However, we note that the location of the Hayashi limit in the H-R diagram is also governed by the convective mixing length (Lucy, Robertson & Sharp 1986). In most stellar models, the Solar value is typically adopted for the mixing length for stars with all masses and metallicities, but recent simulations argue that the mixing length may be dependent on stellar parameters (Trampedach et al. 2014; Magic, Weiss & Asplund 2015). Thus, the Hayashi limit in evolutionary models still needs to be calibrated by observational data.

The target galaxies have different metallicities and thus, our RSG candidates are a good data sample for investigating the metallicity dependence of the effective temperatures of RSGs. Unfortunately, however, our photometric data are not large enough to attempt such an investigation. It is difficult to derive the effective temperatures and bolometric luminosities from our photometric data because of a degeneracy between luminosities, temperatures and circumstellar extinctions, and we do not have spectroscopic data. In this discussion, therefore, we just test the trend of the metallicity dependence of the RSG colour distribution.

Fig. 7 shows the distribution of the $(J - K)_0$ colour distributions of RSGs for the three galaxies. The colour distributions of the genuine RSGs are represented by solid lines, while the histograms for all RSGs (genuine RSGs and possible RSGs) are indicated by dotted lines. The number of RSGs in each bin was divided by the total number of RSGs. The mean colour values for the genuine and all RSGs are indicated by vertical solid and dotted lines, respectively. We could not find a definite progression of the dominant colour towards the bluer colour at a lower metallicity. The peak of the distribution for NGC 5457 seems to be slightly shifted towards the blue colour, but it is not significant. We attribute the absence of a trend in colour with metallicity to the uncertainty in the photometric data. However, it is interesting that recent research into the RSGs in several Local Group galaxies (Davies et al. 2015; Gazak et al. 2015; Patrick et al. 2015) indicates that there is no dependence between the metallicities and temperatures of RSGs. Thus, spectroscopy data are essential for determining the effective temperatures and spectral types of RSGs, from which we can confirm if the changes in spectral type and temperature are caused by metallicity alone or if the RSGs are warmer at lower metallicity.

The mass loss of massive stars is one of the most important parameters in determining their evolutionary itinerary and fate. The dependence of mass-loss rate on metallicity in early-type massive stars has been well established as a power-law dependence ($\propto Z^m$)

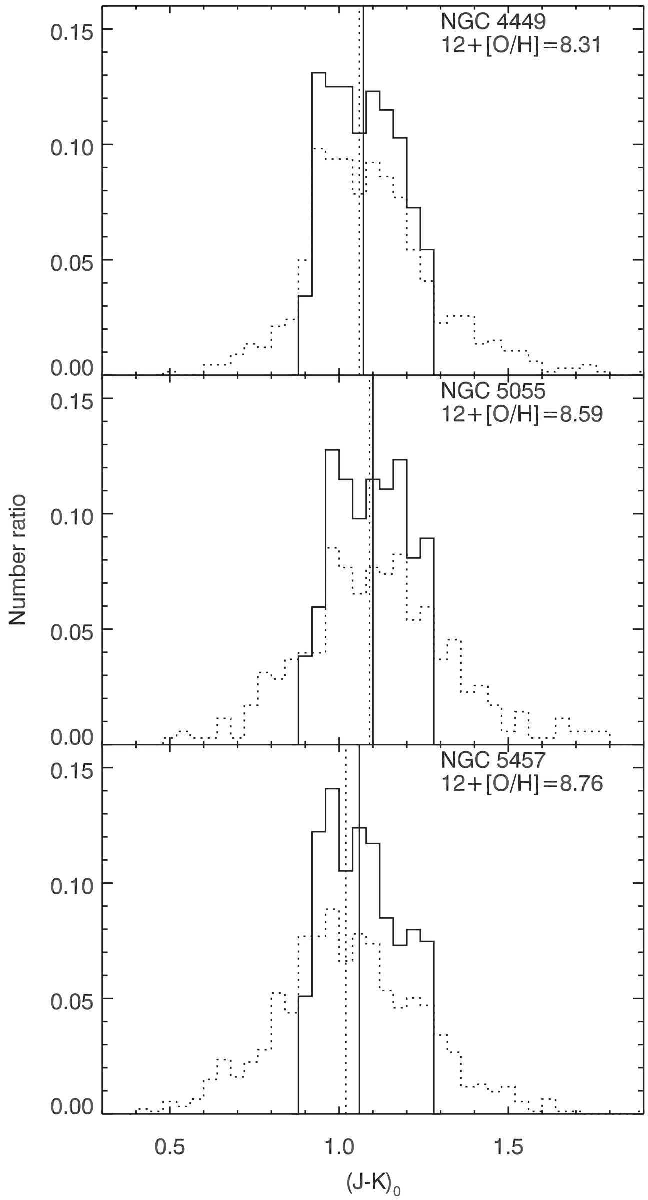

Figure 7. $(J-K)_0$ colour distributions of RSGs for the three galaxies. Solid lines indicate the colour distributions of the genuine RSGs, while the dotted lines are for all RSG candidates (the genuine RSGs and possible RSGs). The mean colour values for the genuine RSGs and all RSGs are described by the vertical solid and dotted lines.

in previous studies (Heger et al. 2003; Mokiem et al. 2007; Puls, Vink & Najarro 2008). Although we still do not know the exact theoretical prediction for the mass-loss rate of RSGs and its dependence on metallicity, Sloan et al. (2008) found that RSGs with lower metallicity have a lower mass-loss rate. Thus, a similar metallicity dependence of mass-loss rate in hot massive stars can be expected for RSGs. If we apply this dependence to RSGs, there is an expectation that metallicity also affects the maximum luminosity of RSGs; the lower metallicity RSGs have higher luminosities. In a higher metallicity domain, the massive stars have a higher mass-loss rate than stars with low metallicity, and this enables lower mass stars to evolve easily into the Wolf–Rayet stage (Massey et al. 2009; Groh, Meynet & Ekström 2013; Levesque 2013; Massey 2013). Consequently, the upper mass limit of RSGs becomes lower with increasing metallicity. Indeed, Massey (1998) detected this relation by measuring the maximum luminosity of RSGs in NGC 6822, M33 and M31.

We compared the brightest absolute magnitudes of the RSGs in the three galaxies. The measured brightest absolute magnitudes for the three galaxies are $M_K = -11.85 \pm 0.01$ for NGC 4449, $M_K = -11.95 \pm 0.01$ for NGC 5055 and $M_K = -11.99 \pm 0.02$ for NGC 5457. We could not find an obvious dependence of the peak magnitude with metallicity. Instead, a similar brightest magnitude of $M_K = -11.9$ was found for the three galaxies. Previously, Massey et al. (2009) compared the maximum luminosities of RSGs in the Milky Way, Magellanic Clouds and M31, and also found that these galaxies share a roughly constant maximum luminosity. The similar brightest magnitude for the three galaxies may be a hint of a constant maximum luminosity (Massey et al. 2009). Therefore, it is essential to derive the exact luminosities for the RSGs of the three galaxies using additional spectroscopy data.

5 SUMMARY

We have investigated the observational properties of RSGs in three nearby galaxies, NGC 4449, NGC 5055 and NGC 5457, using near-infrared *JHK* photometry data obtained from the WFCAM array mounted on the UKIRT. We cross-matched our photometric catalogue with optical archive data and removed foreground Galactic stars and background galaxies from the multi-colour diagrams. The foreground stars can be decoupled from the supergiant populations in the $(i-K, r-i)$ colour–colour diagram in which the foreground stars have large values of the $(r-i)$ colour at a given $(i-K)$. The large values of the $(r-i)$ colour at a given $(i-K)$ for the foreground stars are also described well in the theoretically expected $(i-K, r-i)$ colour–colour diagram calculated by the MARCS model.

The distributions of the RSGs in the $(J-K, K)_0$ CMDs were compared with PARSEC theoretical isochrones. We also investigated the spatial distributions of the RSGs in each galaxy with Hα images, and examined the $(J-K, K)_0$ CMDs of the RSGs in the dominant H II regions of the galaxies. We found that the RSGs of the three galaxies have common ages of $\log(t_{yr}) = 6.9$, 7.1 and 7.3, and that these galaxies have experienced recent star formation within 20 Myr. The maximum age of RSGs in NGC 4449 seems to be about $\log(t_{yr}) = 8.0$ (∼100 Myr), while the upper age limits of RSGs in NGC 5055 and NGC 5457 were not constrained because of the photometric detection limit. NGC 4449 shows distorted and extended spatial distributions of RSGs and has a moderate spatial correlation with the H II regions. The $(J-K, K)_0$ CMD of the central region has more massive and younger stars than other H II regions. NGC 5055 also shows a marginally extended distribution of RSGs, but an exact spatial coherence with the H II regions was not found. We interpret this to mean that the extended distribution of RSGs is likely to be associated with the filament substructures in the outskirts of the galaxy, which are detected in the H I image (Battaglia et al. 2006) and *GALEX* image (Gil de Paz et al. 2007) but not with tidal tails and extended stellar haloes with a red colour (Chonis et al. 2011). NGC 5457 has numerous RSGs younger than the $\log(t_{yr}) = 6.9$ isochrone compared to the other two galaxies, indicating relatively recent star-formation activity in this galaxy. We found that the distribution of RSGs in NGC 5457 has a strong correlation with the H II regions. The CMDs of RSGs in well-known H II regions also indicate that most H II regions in NGC 5457 have not only very young stars but also evolved massive stellar populations.

We examined the effect of metallicity on the colours of the RSGs in the $(J-K, K)_0$ CMD. The $(J-K)_0$ colours of the RSGs in the three galaxies show similar colour distributions, and thus, the expected progression of colours towards higher temperatures with decreasing metallicity was not detected. However, the similar colour distributions in the three galaxies does reflect the recent observational results of no dependence between metallicities and temperatures of RSGs found for several Local Group galaxies. We could not confirm the relation between maximum luminosity and metallicity that was suggested by Massey (1998). Instead, we found that the three galaxies shared a similar brightest absolute magnitude of $M_K = -11.9$.

Overall, in this study we hope to provide RSG candidates from the three galaxies for future RSG studies using large telescopes. A photometric study of supergiant stars alone is limited. Therefore, follow-up spectroscopic observations are necessary for investigating the metallicity dependence of the RSGs as well as determining the spectral types and extinction values. We expect that an updated methodology, such as the SED fitting method of Davies et al. (2013), will provide more obvious results for the physical properties of RSGs in nearby galaxies, and we also plan to extend our work for the three galaxies using spectroscopic data.

ACKNOWLEDGEMENTS

We are grateful to the anonymous referee for detailed comments that greatly improved this paper. This research was supported by the Basic Science Research Program through the National Research Foundation of Korea (NRF) funded by the Ministry of Education, Science and Technology (NRF-2015R1A6A3A03016141). YJS is also grateful for the support of the Basic Science Research Program (NRF-2016R1D1A1B01006608). This paper is based in part on data collected by the Subaru Telescope and obtained from SMOKA, which is operated by the Astronomy Data Center, National Astronomical Observatory of Japan. It uses observations obtained with MegaPrime/MegaCam, a joint project of the Canada-France-Hawaii Telescope (CFHT) and CEA/IRFU at the CFHT, which is operated by the National Research Council of Canada (NRC), the Institut National des Science de l'Univers of the Centre National de la Recherche Scientifique (CNRS) of France and the University of Hawaii. This work is based in part on data products produced at Terapix and made available from the Canadian Astronomy Data Centre as part of the Canada-France-Hawaii Telescope Legacy Survey, a collaborative project of NRC and CNRS.

REFERENCES

Annibali F., Aloisi A., Mack J., Tosi M., van der Marel R. P., Angeretti L., Leitherer C., Sirianni M., 2008, AJ, 135, 1900
Annibali F., Tosi M., Aloisi A., van der Marel R. P., Martinez-Delgado D., 2012, ApJ, 745, L1
Baba H. et al., 2002, in Bohlender D. A., Durand D., Handley T. H., eds, ASP Conf. Ser. Vol. 281, Astronomical Data Analysis Software and Systems XI. Astron. Soc. Pac., San Francisco, p. 298
Battaglia G., Fraternali F., Oosterloo T., Sancisi R., 2006, A&A, 447, 49
Bertin E., Mellier Y., Radovich M., Missonnier G., Didelon P., Morin B., 2002, in Bohlender D. A., Durand D., Handley T. H., eds, ASP Conf. Ser. Vol. 281, Astronomical Data Analysis Software and Systems XI. Astron. Soc. Pac., San Francisco, p. 228
Bressan A., Marigo P., Girardi L., Salasnich B., Dal Cero C., Rubele S., Nanni A., 2012, MNRAS, 427, 127
Bressan A., Marigo P., Girardi L., Nanni A., Rubele S., 2013, European Phys. J. Web Conf. p. 03001
Casagrande L., VandenBerg D. A., 2014, MNRAS, 444, 392
Charbonnel C., Meynet G., Maeder A., Schaller G., Schaerer D., 1993, A&AS, 101, 415
Chonis T. S., Martínez-Delgado D., Gabany R. J., Majewski S. R., Hill G. J., Gralak R., Trujillo I., 2011, AJ, 142, 166
Cohen M., Wheaton W. A., Megeath S. T., 2003, AJ, 126, 1090
Dale D. A. et al., 2009, ApJ, 703, 517
Davidge T. J., 2010, ApJ, 725, 1342
Davies B. et al., 2013, ApJ, 767, 3
Davies B., Kudritzki R.-P., Gazak Z., Plez B., Bergemann M., Evans C., Patrick L., 2015, ApJ, 806, 21
Doi M. et al., 2010, AJ, 139, 1628
Drout M. R., Massey P., Meynet G., 2012, ApJ, 750, 97
Dye S. et al., 2006, MNRAS, 372, 1227
Elias J. H., Frogel J. A., Humphreys R. M., 1985, ApJS, 57, 91
Garnett D. R., Kennicutt R. C. Jr., 1994, ApJ, 426, 123
Gazak J. Z. et al., 2015, ApJ, 805, 182
Gil de Paz A. et al., 2007, ApJS, 173, 185
Grammer S., Humphreys R. M., 2013, AJ, 146, 114
Groh J. H., Meynet G., Ekström S., 2013, A&A, 550, L7
Gustafsson B., Edvardsson B., Eriksson K., Mizuno-Wiedner M., Jørgensen U. G., Plez B., 2003, in Hubeny I., Mihalas D., Werner K., eds, ASP Conf. Ser. Vol. 288, Stellar Atmosphere Modeling. Astron. Soc. Pac., San Francisco, p. 331
Gustafsson B., Edvardsson B., Eriksson K., Jørgensen U. G., Nordlund Å., Plez B., 2008, A&A, 486, 951
Hartmann L. W., Geller M. J., Huchra J. P., 1986, AJ, 92, 1278
Hayashi C., Hoshi R., 1961, PASJ, 13, 442
Heger A., Fryer C. L., Woosley S. E., Langer N., Hartmann D. H., 2003, ApJ, 591, 288
Hill R. S. et al., 1998, ApJ, 507, 179
Humphreys R. M., 1979, ApJ, 231, 384
Hunter D. A., Gallagher J. S., III, 1997, ApJ, 475, 65
Hunter D. A., Gallagher J. S., Rautenkranz D., 1982, ApJS, 49, 53
Hunter D. A., Wilcots E. M., van Woerden H., Gallagher J. S., Kohle S., 1998, ApJ, 495, L47
Jordi K., Grebel E. K., Ammon K., 2006, A&A, 460, 339
Karachentsev I. D., Karachentseva V. E., Huchtmeier W. K., 2007, Astron. Lett., 33, 512
Kennicutt R. C. Jr., Bresolin F., Garnett D. R., 2003, ApJ, 591, 801
Kennicutt R. C. Jr., Lee J. C., Funes José G. S. J., Sakai S., Akiyama S., 2008, ApJS, 178, 247
Leroy A. K. et al., 2009, AJ, 137, 4670
Levesque E. M., 2013, in Kervella P., Le Bertre T., Perrin G., eds, EAS Publ. Ser. Vol. 60, p. 269
Levesque E. M., Massey P., Olsen K. A. G., Plez B., Josselin E., Maeder A., Meynet G., 2005, ApJ, 628, 973
Levesque E. M., Massey P., Olsen K. A. G., Plez B., Meynet G., Maeder A., 2006, ApJ, 645, 1102
Lucy L. B., Robertson J. A., Sharp C. M., 1986, A&A, 154, 267
Maeder A., 1981, A&A, 101, 385
Maeder A., Meynet G., 2001, A&A, 373, 555
Magic Z., Weiss A., Asplund M., 2015, A&A, 573, A89
Martin C. L., 1997, ApJ, 491, 561
Martínez-Delgado D. et al., 2012, ApJ, 748, L24
Massey P., 1998, ApJ, 501, 153
Massey P., 2003, ARA&A, 41, 15
Massey P., 2013, New Astron. Rev., 57, 14
Massey P., Olsen K. A. G., 2003, AJ, 126, 2867
Massey P., Plez B., Levesque E. M., Olsen K. A. G., Clayton G. C., Josselin E., 2005, ApJ, 634, 1286
Massey P., Silva D. R., Levesque E. M., Plez B., Olsen K. A. G., Clayton G. C., Meynet G., Maeder A., 2009, ApJ, 703, 420
Matheson T. et al., 2012, ApJ, 754, 19
Meynet G., Maeder A., 2005, A&A, 429, 581
Mokiem M. R. et al., 2007, A&A, 473, 603
Neugent K. F., Massey P., Skiff B., Meynet G., 2012, ApJ, 749, 177
Patrick L. R., Evans C. J., Davies B., Kudritzki R.-P., Gazak J. Z., Bergemann M., Plez B., Ferguson A. M. N., 2015, ApJ, 803, 14

Pierce M. J., 1994, ApJ, 430, 53
Pilyugin L. S., Thuan T. X., 2005, ApJ, 631, 231
Plez B., 2003, in Munari U., ed., ASP Conf. Ser. Vol. 298, GAIA Spectrosc.: Sci. Technol. Astron. Soc. Pac., San Francisco, p. 189
Puls J., Vink J. S., Najarro F., 2008, A&AR, 16, 209
Rosa M. R., Benvenuti P., 1994, A&A, 291, 1
Rozas M., 2008, RMxAA, 44, 161
Sargent B. A., Srinivasan S., Meixner M., 2011, ApJ, 728, 93
Schaller G., Schaerer D., Meynet G., Maeder A., 1992, A&AS, 96, 269
Schlafly E. F., Finkbeiner D. P., 2011, ApJ, 737, 103
Searle L., 1971, ApJ, 168, 327
Sedwick K. E., Aller L. H., 1981, Proc. Natl. Acad. Sci., 78, 1994
Shappee B. J., Stanek K. Z., 2011, ApJ, 733, 124
Sloan G. C., Kraemer K. E., Wood P. R., Zijlstra A. A., Bernard-Salas J., Devost D., Houck J. R., 2008, ApJ, 686, 1056
Stetson P. B., 1987, PASP, 99, 191
Stetson P. B., Harris W. E., 1988, AJ, 96, 909
Talent D. L., 1980, PhD thesis, Rice Univ., Houston, TX
Thilker D. A. et al., 2007, ApJS, 173, 538
Thronson H. A. Jr., Hunter D. A., Telesco C. M., Harper D. A., Decher R., 1987, ApJ, 317, 180
Trampedach R., Stein R. F., Christensen-Dalsgaard J., Nordlund Å., Asplund M., 2014, MNRAS, 445, 4366
Tully R. B., Rizzi L., Shaya E. J., Courtois H. M., Makarov D. I., Jacobs B. A., 2009, AJ, 138, 323
van der Hulst T., Sancisi R., 1988, AJ, 95, 1354
van der Kruit P. C., 1979, A&AS, 38, 15
Verhoelst T., van der Zypen N., Hony S., Decin L., Cami J., Eriksson K., 2009, A&A, 498, 127
Vink J. S., de Koter A., Lamers H. J. G. L. M., 2001, A&A, 369, 574
Vinkó J. et al., 2012, A&A, 546, A12
Waller W. H. et al., 1997, ApJ, 481, 169
Walter F., Brinks E., de Blok W. J. G., Bigiel F., Kennicutt R. C. Jr., Thornley M. D., Leroy A., 2008, AJ, 136, 2563

This paper has been typeset from a TEX/LATEX file prepared by the author.